LETTER

doi:10.1038/nature09393

# Spin–imbalance in a one-dimensional Fermi gas

Yean-an Liao[1]*, Ann Sophie C. Rittner[1]*, Tobias Paprotta[1], Wenhui Li[1,3], Guthrie B. Partridge[1]†, Randall G. Hulet[1], Stefan K. Baur[2] & Erich J. Mueller[2]

**Superconductivity and magnetism generally do not coexist. Changing the relative number of up and down spin electrons disrupts the basic mechanism of superconductivity, where atoms of opposite momentum and spin form Cooper pairs. Nearly forty years ago Fulde and Ferrell[1] and Larkin and Ovchinnikov[2] (FFLO) proposed an exotic pairing mechanism in which magnetism is accommodated by the formation of pairs with finite momentum. Despite intense theoretical and experimental efforts, however, polarized superconductivity remains largely elusive[3]. Unlike the three-dimensional (3D) case, theories predict that in one dimension (1D) a state with FFLO correlations occupies a major part of the phase diagram[4–12]. Here we report experimental measurements of density profiles of a two-spin mixture of ultracold $^6$Li atoms trapped in an array of 1D tubes (a system analogous to electrons in 1D wires). At finite spin imbalance, the system phase separates with an inverted phase profile, as compared to the 3D case. In 1D, we find a partially polarized core surrounded by wings which, depending on the degree of polarization, are composed of either a completely paired or a fully polarized Fermi gas. Our work paves the way to direct observation and characterization of FFLO pairing.**

The FFLO states are perhaps the most interesting of a number of exotic polarized superconducting phases proposed in the past 40 years. In the original concept of Fulde and Ferrell, Cooper pairs form with finite centre-of-mass momentum[1]. Larkin and Ovchinnikov proposed a related model in which the superconducting order parameter oscillates in space[2]. These two ideas are closely related, because the oscillating order parameter may be interpreted as an interference pattern between condensates with opposite centre-of-mass momenta. The spin density oscillates in the Larkin and Ovchinnikov model, leading to a build-up of polarization in the nodes of the superconducting order parameter. Thus, the Larkin and Ovchinnikov state can be considered a form of microscale phase separation with alternating superfluid and polarized normal regions. By including more and more momenta, subsequent theorists were able to evaluate the stability of ever more complicated spatial structures[3].

Previous studies of superfluidity in fermionic atoms show that ultracold atoms form a powerful tool with which to investigate the emergent properties of interacting systems of many particles. Although they are largely analogous to an electronic superconductor, the atomic systems feature tunable interactions. This extra degree of control has led to a number of unique experiments and conceptual advances. Furthermore, the absence of spin relaxation enables us to spin-polarize the atoms to explore the interplay between magnetism and superfluidity, with the potential to observe the FFLO phase. Recent calculations indicate that if a FFLO phase exists in 3D trapped gases, it will occupy a very small volume in parameter space[13,14]. Experiments in 3D and in the strongly interacting limit show that the gas phase separates with an unpolarized superfluid core surrounded by a polarized shell[15–19], with no evidence for the FFLO phase. Here, we study a polarized Fermi gas in 1D, for which theory predicts that a large fraction of the phase diagram is occupied by an FFLO-like phase (see Fig. 1a)[4–12]. In this 1D setting, the physics should be closest to that described by Larkin and Ovchinnikov, where an oscillating superfluid order parameter coexists with a spin-density wave. Owing to fluctuations, the order will be algebraic rather than long-range. The increased stability of FFLO-like phases in 1D can be understood as a 'nesting' effect, in which a single wavevector connects all points on the Fermi surface, allowing all atoms on the Fermi surface to participate in finite momentum pairing, whereas in 3D, only a small fraction of these atoms are able to do so. Similar enhancements are predicted for systems of lattice fermions and quasi-1D geometries[10,20].

Our work complements studies of astrophysical objects[3] and solid-state systems. Like our current experiment, the solid-state experiments

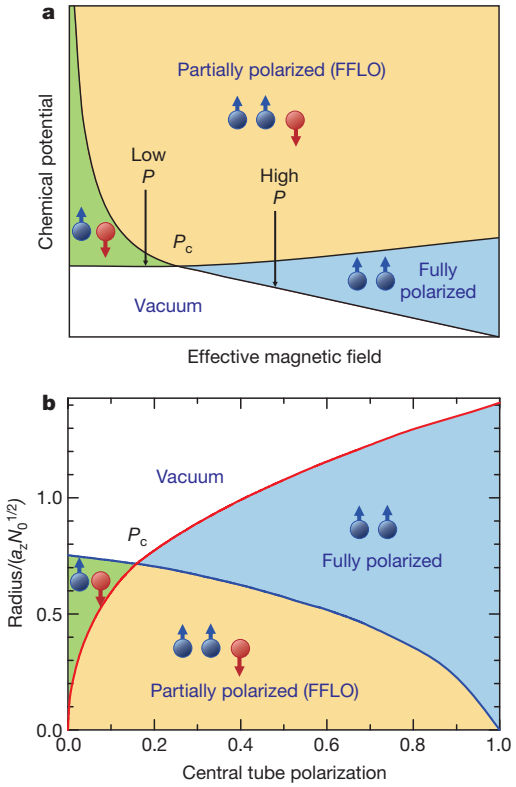


**Figure 1 | Theoretical $T = 0$ phase diagram (adapted from ref. 6).** **a**, Schematic with $\mu = \frac{1}{2}(\mu_1 + \mu_2)$ versus $h = \frac{1}{2}(\mu_1 - \mu_2)$, showing three phases: fully paired (green), fully polarized (blue), and partially polarized (yellow), which is predicted to be FFLO. In a trap, $\mu$ decreases from the centre to the edge, while $h$ is constant throughout the tube. The vertical arrows show two possible paths from the trap centre to edge: The partially polarized centre is surrounded either by a fully paired superfluid phase at low $h$ or by a fully polarized phase at high $h$. At a critical value of $h$, corresponding to a polarization $P_c$, the whole cloud is partially polarized. **b**, Phase diagram of the 1D trapped gas with infinitely strong point interactions. The scaled axial radius is defined in the Fig. 3 caption. The red line corresponds to the scaled radius of the density difference, and the blue line is the scaled radius of state $|2\rangle$.

[1]Department of Physics and Astronomy and Rice Quantum Institute, Rice University, Houston, Texas 77251, USA. [2]Laboratory of Atomic and Solid State Physics, Cornell University, Ithaca, New York 14853, USA. [3]Centre for Quantum Technologies, National University of Singapore, 3 Science Drive 2, 117543 Singapore. †Present address: Laboratoire Charles Fabry de l'Institut d'Optique, UMR CNRS 8501, Palaiseau, France.

*These authors contributed equally to this work.

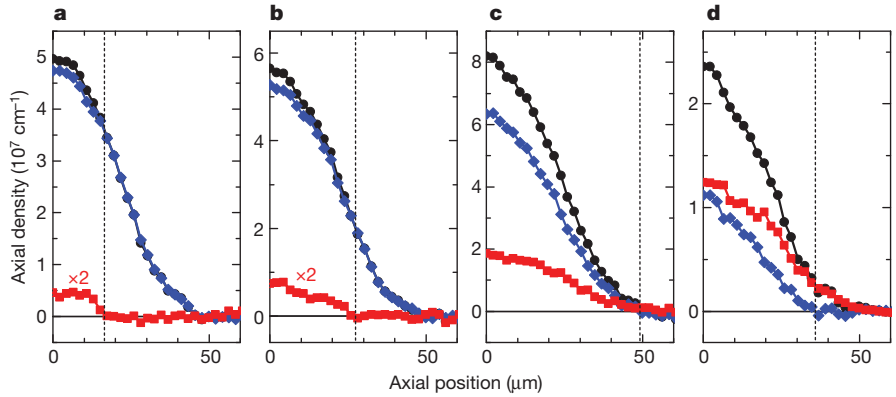


**Figure 2 | Axial density profiles of a spin-imbalanced 1D ensemble of tubes.** Integrated axial density profiles of the tube bundles (black circles represent the majority, the blue diamonds represent the minority, and the red squares show the difference) are shown as functions of central $P$. **a**, At low $P$ (=0.015), the edge of the cloud is fully paired and the density difference is zero. The centre of the cloud is partially polarized. The density difference has been multiplied by two for better visibility of the phase boundary (dashed black line). **b**, For increasing $P$ (=0.055), the phase boundary moves to the edge of the cloud as the partially polarized region grows. **c**, Near $P_c$ ($P$ =0.10), where almost the entire cloud is partially polarized. **d**, Well above $P_c$ ($P$ =0.33), where the edge of the cloud is fully polarized and the minority density vanishes.

typically involve highly anisotropic materials—made up either of weakly coupled two-dimensional (2D) planes or 1D wires. Examples include the organic superconductor λ-$(BETS)_2FeCl_4$ (ref. 21) and the heavy fermion superconductor $CeCoIn_5$ (refs 22 and 23). However, FFLO states have not been conclusively observed in any system.

Details of our experimental procedures are given in the Methods and in refs 16 and 17. We create a mixture of the two lowest hyperfine levels of the $^6$Li ground state, the majority state $|1\rangle$, and the minority state $|2\rangle$. An array of 1D tubes is formed with a 2D optical lattice[24]. The lattice potential is given by $V = V_0\cos^2(kx) + V_0\cos^2(ky)$, with $k = 2\pi/\lambda$ and $V_0 = 12\varepsilon_r$, where $V_0$ is the potential depth, $x$ and $y$ are two orthogonal radial coordinates, $\lambda$ is the optical trap laser wavelength of 1,064 nm, $\varepsilon_r = \hbar^2k^2/2m$ is the recoil energy, and $m$ is the mass of a $^6$Li atom. There are several requirements to be met for the system to be 1D. First, only the lowest transverse mode in each tube may be populated. This requires that both the thermal energy $k_BT$ and the 1D Fermi energy $\varepsilon_F = N_1\hbar\omega_z$ be small compared to the transverse confinement energy $\hbar\omega_\perp$. Here $N_1$ is the number of atoms per 1D tube in state $|1\rangle$, and $\omega_z$ and $\omega_\perp$ are the axial and transverse confinement frequencies of an individual tube. Second, the single-particle tunnelling rate $t$ should be small compared to both $\varepsilon_F$ and $T$. The condition $\varepsilon_F > t$ is equivalent to specifying that the Fermi surface is 1D, and the condition $T > t$ makes the inter-tube coupling incoherent. All conditions are well satisfied in our experiment: the tube aspect ratio $\omega_\perp/\omega_z = 1{,}000$ is larger than $N_1 \approx 120$ for the central tube; and $t/k_B \approx 17$ nK is much smaller than both $\varepsilon_F/k_B \approx 1.2$ μK and $T \approx 175$ nK.

We tune an external magnetic field to the Bardeen–Cooper–Schrieffer (BCS) side (890 G) of the broad 3D Feshbach resonance in $^6$Li (refs 25 and 26), where the 1D interactions are strongly attractive[27,28]. We measure the *in situ* density of the two spin species by sequential imaging with two probe laser beams, choosing their intensity and frequency to maximize the signal-to-noise ratio of the density difference (see Methods). Assuming hydrostatic equilibrium, the 1D spatial density profiles $n_{1,2}(z)$ can be expressed in terms of $\mu = \mu_0 - V(z)$, and $h = h_0$, where $\mu_0$ and $h_0$ are the chemical potential and chemical potential difference at the centre of the tube, set by the total number of particles in the tube $N = N_1 + N_2$ and polarization $P = (N_1 - N_2)/N$; $V(z)$ is the axial confinement potential. In particular, the phase boundary between the fully paired and partially polarized regions occurs where the density difference $n_1(z) - n_2(z) = 0$, and the boundary between the fully and partially polarized phases corresponds to $n_2(z) = 0$, as shown in Fig. 1b.

Figure 2 shows axial density profiles of state $|1\rangle$, state $|2\rangle$, and their differences for a range of polarizations. These images represent the sum of the linear density in all tubes in our system, and are produced by integrating our column density images across the remaining transverse direction. At low polarization, a partially polarized region forms at the centre of the trap (Fig. 2a), the radius of which increases with increasing polarization (Fig. 2b). This is distinctly different from a polarized 3D gas in which the centre is fully paired. At a critical polarization $P_c$, the partially polarized region extends to the edge of the cloud (Fig. 2c). When the polarization increases further, the edge of the cloud becomes fully polarized (Fig. 2d). From the images of the atomic clouds we extract the axial radii of the ensemble of tubes of the minority density and the density difference. The axial radii of the tube bundle are equivalent to the central tube radius for our experiment because the inner and outer boundaries both decrease monotonically going from the central to the outer tubes (see Supplementary Information). We perform an inverse Abel transform to obtain the number of particles and polarization in the central tube. Following ref. 6, we plot these radii as a function of the central tube polarization (Fig. 3), normalizing the radii by $(N_0)^{1/2}a_z$, where $N_0$ is the total number of particles in the central tube and $a_z = (\hbar/m\omega_z)^{1/2}$ is the harmonic oscillator length along the central tube. The critical polarization $P_c$ corresponds to the crossing of these two radii where the entire cloud is

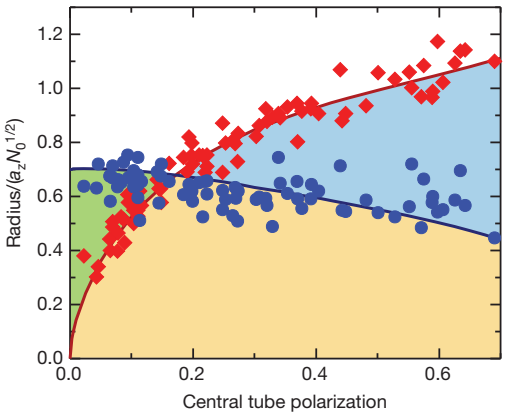


**Figure 3 | Experimental phase diagram as a function of polarization in the central tube.** The scaled radii of the axial density difference (red diamonds) and the minority state ($|2\rangle$) axial density (blue circles) compared with a 175 nK Bethe ansatz calculation (solid lines). The dimensionless scaled axial radius $R/(a_zN_0^{1/2})$ is plotted, where $R$ is the position along the bundle of tubes where the respective density vanishes, $N_0$ is the total number of particles in the central tube, and $a_z$ is the axial harmonic confinement length. At $P \approx 0.13 \pm 0.03$, both radii intersect, indicating that the entire cloud is partially polarized. The data are in reasonable agreement with the theoretical crossing at slightly higher polarization $P \approx 0.17$.

partially polarized: for $P < P_c$ the radius of the density difference is smaller than the minority radius, while the opposite occurs for $P > P_c$. From a linear fit to the data, we find $P_c = 0.13 \pm 0.03$. We use the thermodynamic Bethe ansatz to calculate theoretical density distributions, and carry out an identical analysis. We find quantitative agreement with the experimental density profiles, with a best-fit temperature of $T = 175 \pm 50\,\mathrm{nK} = 0.15T_F$ (see Supplementary Information). The theoretical density profiles yield $P_c = 0.17$ with weak temperature dependence.

Although these density profiles do not directly reveal FFLO correlations, the theoretical consensus is that such correlations should be present. For example, mean-field calculations[29] predict that at $T = 0.15T_F$, there should be a range of polarizations near $P_c$ that yield detectable FFLO order. Our stronger interactions should make the low-temperature phases even more robust[11].

We have created a strongly interacting, two-component Fermi gas in 1D and measured its phase diagram as a function of polarization. The system is at sufficiently low temperature to observe three distinct phases, in agreement with theory. This is an example of an optical lattice-based quantum simulator that produces a phase diagram of non-trivial quantum phases. Although we have not directly observed the FFLO phase, the observed density profiles agree quantitatively with theories that exhibit the 1D equivalent of FFLO correlations at low temperature[11,29]. In the future, we intend to measure the pair momentum distribution of the partially polarized phase to reveal its non-zero pair momentum directly.

## METHODS SUMMARY

We start from quantum degenerate, spin-imbalanced $^6$Li Fermi gas in a single-beam far-off-resonance optical trap[16,17], which is then loaded into a crossed-beam optical dipole trap formed by a pair of retro-reflected beams propagating in the $x$ and $y$ directions. We turn on the 2D lattice by ramping up the optical trap laser power and rotating the polarizations of the retro-reflected beams to create standing waves in two orthogonal directions. The intersection of the standing waves creates 1D tubes with an energy depth of $12\varepsilon_r$ in the central tube, with $\omega_\perp = (2\pi)\,2 \times 10^5$ Hz and $\omega_z = (2\pi)\,200$ Hz. At a global polarization $P \approx 0$, the total number of atoms is $\sim 4 \times 10^5$, giving a total number of atoms in the central tube of $N \approx 240 \pm 20$. The column densities of each state and their difference is obtained from two *in situ* polarization phase contrast images[30] taken in rapid succession and with different detuning. The temperature is determined by fitting the *in situ* density of a balanced spin mixture to a Thomas–Fermi distribution and is measured to be $T < 0.05T_F$ before turning on the 2D lattice and $T \approx 0.09 \pm 0.03T_F$ after slowly turning on the lattice and then slowly rotating the polarization back to the 3D trap configuration. The temperature in the lattice is estimated from the *in situ* density distributions.

**Full Methods** and any associated references are available in the online version of the paper at www.nature.com/nature.

**Received 3 May; accepted 3 August 2010.**


1. Fulde, P. & Ferrell, R. A. Superconductivity in a strong spin-exchange field. *Phys. Rev.* **135,** A550–A563 (1964).
2. Larkin, A. I. & Ovchinnikov, Y. N. Inhomogeneous state of superconductors. *Sov. Phys. JETP* **20,** 762–769 (1965).
3. Casalbuoni, R. & Nardulli, G. Inhomogeneous superconductivity in condensed matter and QCD. *Rev. Mod. Phys.* **76,** 263–320 (2004).
4. Yang, K. Inhomogeneous superconducting state in quasi-one-dimensional systems. *Phys. Rev. B* **63,** 140511(R) (2001).
5. Mizushima, T., Machida, K. & Ichioka, M. Direct imaging of spatially modulated superfluid phases in atomic fermion systems. *Phys. Rev. Lett.* **94,** 060404 (2005).
6. Orso, G. Attractive Fermi gases with unequal spin populations in highly elongated traps. *Phys. Rev. Lett.* **98,** 070402 (2007).
7. Hu, H., Liu, X.-J. & Drummond, P. D. Phase diagram of a strongly interacting polarized Fermi gas in one dimension. *Phys. Rev. Lett.* **98,** 070403 (2007).
8. Guan, X. W., Batchelor, M. T., Lee, C. & Bortz, M. Phase transitions and pairing signature in strongly attractive Fermi atomic gases. *Phys. Rev. B* **76,** 085120 (2007).
9. Feiguin, A. E. & Heidrich-Meisner, F. Pairing states of a polarized fermi gas trapped in a one-dimensional optical lattice. *Phys. Rev. B* **76,** 220508 (2007).
10. Parish, M. M., Baur, S. K., Mueller, E. J. & Huse, D. A. Quasi-one-dimensional polarized Fermi superfluids. *Phys. Rev. Lett.* **99,** 250403 (2007).
11. Casula, M., Ceperley, D. M. & Mueller, E. J. Quantum Monte Carlo study of one-dimensional trapped fermions with attractive contact interactions. *Phys. Rev. A* **78,** 033607 (2008).
12. Kakashvili, P. & Bolech, C. J. Paired states in spin-imbalanced atomic Fermi gases in one dimension. *Phys. Rev. A* **79,** 041603 (2009).
13. Sheehy, D. E. & Radzihovsky, L. BEC-BCS crossover, phase transitions and phase separation in polarized resonantly-paired superfluids. *Ann. Phys.* **322,** 1790–1924 (2007).
14. Bulgac, A. & Forbes, M. M. Unitary Fermi supersolid: the Larkin-Ovchinnikov phase. *Phys. Rev. Lett.* **101,** 215301 (2008).
15. Zwierlein, M. W., Schirotzek, A., Schunck, C. H. & Ketterle, W. Fermionic superfluidity with imbalanced spin populations. *Science* **311,** 492–496 (2006).
16. Partridge, G. B., Li, W., Kamar, R. I., Liao, Y.-a. & Hulet, R. G. Pairing and phase separation in a polarized Fermi gas. *Science* **311,** 503–505 (2006).
17. Partridge, G. B. *et al.* Deformation of a trapped Fermi gas with unequal spin populations. *Phys. Rev. Lett.* **97,** 190407 (2006).
18. Shin, Y.-I., Schunck, C. H., Schirotzek, A. & Ketterle, W. Phase diagram of a two-component Fermi gas with resonant interactions. *Nature* **451,** 689–693 (2008).
19. Nascimbène, S. *et al.* Collective oscillations of an imbalanced Fermi gas: axial compression modes and polaron effective mass. *Phys. Rev. Lett.* **103,** 170402 (2009).
20. Zhao, E. & Liu, W. V. Theory of quasi-one-dimensional imbalanced Fermi gases. *Phys. Rev. A* **78,** 063605 (2008).
21. Uji, S. *et al.* Vortex dynamics and the Fulde-Ferrell-Larkin-Ovchinnikov state in a magnetic-field-induced organic superconductor. *Phys. Rev. Lett.* **97,** 157001 (2006).
22. Radovan, H. *et al.* Magnetic enhancement of superconductivity from electron spin domains. *Nature* **425,** 51–55 (2003).
23. Kenzelmann, M. *et al.* Coupled superconducting and magnetic order in $CeCoIn_5$. *Science* **321,** 1652–1654 (2008).
24. Moritz, H., Stöferle, T., Günter, K., Köhl, M. & Esslinger, T. Confinement induced molecules in a 1D Fermi gas. *Phys. Rev. Lett.* **94,** 210401 (2005).
25. Houbiers, M., Stoof, H. T. C., McAlexander, W. I. & Hulet, R. G. Elastic and inelastic collisions of $^6$Li atoms in magnetic and optical traps. *Phys. Rev. A* **57,** R1497–R1500 (1998).
26. Bartenstein, M. *et al.* Precise determination of $^6$Li cold collision parameters by radio-frequency spectroscopy on weakly bound molecules. *Phys. Rev. Lett.* **94,** 103201 (2005).
27. Tokatly, I. V. Dilute Fermi gas in quasi-one-dimensional traps: from weakly interacting fermions via hard core bosons to a weakly interacting Bose gas. *Phys. Rev. Lett.* **93,** 090405 (2004).
28. Fuchs, J. N., Recati, A. & Zwerger, W. Exactly solvable model of the BCS-BEC crossover. *Phys. Rev. Lett.* **93,** 090408 (2004).
29. Liu, X.-J., Hu, H. & Drummond, P. D. Finite-temperature phase diagram of a spin-polarized ultracold Fermi gas in a highly elongated harmonic trap. *Phys. Rev. A* **78,** 023601 (2008).
30. Bradley, C. C., Sackett, C. A. & Hulet, R. G. Bose-Einstein condensation of lithium: observation of limited condensate number. *Phys. Rev. Lett.* **78,** 985–989 (1997).


**Supplementary Information** is linked to the online version of the paper at www.nature.com/nature.

**Acknowledgements** We thank S. E. Pollack for providing software to remove fringes from the images and M. Revelle for help on the experiment. E.J.M. would like to thank C. Bolech and P. Kakashvili for discussion of techniques for analysing the data. This work was supported under ARO Award W911NF-07-1-0464 with funds from the DARPA OLE programme, and by the NSF, the ONR, the Welch Foundation (grant C-1133) and the Keck Foundation.

**Author Contributions** Y.-a.L., T.P., A.S.C.R., G.B.P., W.L. and R.G.H. constructed the apparatus. Y.-a.L., A.S.C.R. and T.P. acquired and processed the data. S.K.B. and E.J.M. did the theory and extracted the phase boundaries from the data. R.G.H and E.J.M. supervised the investigation. All authors contributed to writing the manuscript.

**Author Information** Reprints and permissions information is available at www.nature.com/reprints. The authors declare no competing financial interests. Readers are welcome to comment on the online version of this article at www.nature.com/nature. Correspondence and requests for materials should be addressed to R.G.H. (randy@rice.edu).

## METHODS

**Preparation.** We produce a quantum degenerate, strongly interacting, spin-imbalanced $^6$Li Fermi gas using our previously published methods[16,17]. Starting from a quantum degenerate gas of $^6$Li in a single-beam far-off-resonance optical dipole trap, we control the relative population of two hyperfine states, $F = 1/2$, $m_F = 1/2$ (state $|1\rangle$) and $F = 1/2$, $m_F = -1/2$ (state $|2\rangle$), where $F$ is the total spin and $m_F$ is the projection along the quantization axis, by driving radio-frequency sweeps between them at different powers. The spin mixture is created in a uniform magnetic field at 765 G within the broad Feshbach resonance between states $|1\rangle$ and $|2\rangle$ centred at 834 G (refs 25 and 26). Atoms are evaporatively cooled by lowering the trap depth in the single-beam optical trap. During evaporation, the field is adiabatically swept to 890 G, on the BCS side of the Feshbach resonance, where the 3D scattering length $a_{3D} = -9145a_o$ ($a_o$ is the Bohr radius). At the end of evaporation, we turn on a crossed-beam optical dipole trap formed by two orthogonal, retro-reflected laser beams, with elliptical laser-beam waists ($1/e^2$ radii) of 54 μm by 236 μm, with the beams propagating in the $x$–$y$ plane and the long axes of the ellipses oriented along $z$. The polarization of each retro-reflected beam is controlled by liquid crystal variable retarders and is perpendicular to that of the incident beam in the trap configuration. The trap depth is 0.5 μK with axial and radial trapping frequencies of 50 Hz and 153 Hz, respectively. We then turn on the optical lattice by simultaneously ramping up the laser power and rotating the polarization of each retro beam to be parallel to its corresponding incident beam, resulting in a 2D lattice of 1D tubes. The lattice turn-on time constants are 130 ms for intensity and 70 ms for polarization, with both having smooth error-function-like trajectories, optimized to minimize heating. The final 1D lattice depth is $12\varepsilon_r$ ($\varepsilon_r = 1.39$ μK) with radial and axial trapping frequencies in the central tube of $\omega_\perp = (2\pi)2 \times 10^5$ Hz and $\omega_z = (2\pi)200$ Hz, respectively. After waiting 50 ms, we take images that record the column densities of each state in the array of 1D tubes. Under these conditions $a_\perp = 1{,}720a_o$, $a_z = 5.3 \times 10^4 a_o$, and $a_{1D} = 2099a_o$, where $a_{\perp,z} = (\hbar/m\omega_{\perp,z})^{1/2}$ and $a_{1D}$ is the 1D scattering length defined in ref. 31.

**Imaging.** The column densities of each state and their difference is obtained from two *in situ* phase-contrast polarization imaging[30] shots, taken in rapid succession and with different detunings near the $^2S_{1/2}$ to $^2P_{3/2}$ atomic transition. Imaging 1D gases *in situ* is problematic owing to high optical densities and heating from the first laser pulse. The first pulse dissociates atom pairs and the release of binding energy affects the second image. At 890 G, the binding energy in 1D is ~6 μK, whereas in 3D this field corresponds to the BCS limit where there is little pairing energy. To minimize heating effects in the second image we use phase-contrast polarization imaging with short intervals (as short as 5 μs) between images (see Supplementary Information for more imaging details).

**Temperature.** In the absence of the optical lattice an effective temperature is measured by fitting finite-temperature Thomas–Fermi distributions to clouds prepared with $P = 0$ (refs 16 and 32). Before turning on the lattice, the effective temperature is $<0.05T_F$ in the shallow trap, where $T_F$ is the Fermi temperature of a non-interacting gas of $N_1$ fermions[16]. In the lattice, temperature is measured by comparing the experimental column densities with the theory described in the next section.

**The spin-imbalanced attractive 1D gas.** Sufficiently far from the confinement-induced resonance on its attractive side, the 1D spin-imbalanced attractively interacting Fermi gas may be described by the exactly solvable Gaudin–Yang model[33,34,35] with the Hamiltonian

$$H = \sum_{\sigma=1,2}\sum_{i=1}^{N_\sigma}\frac{p_{i\sigma}^2}{2m} + g_{1D}\sum_{i=1}^{N_1}\sum_{j=1}^{N_2}\delta(z_{i1}-z_{j2})$$

where the 1D coupling constant is related to the 1D scattering length by $g_{1D} = -\dfrac{2\hbar^2}{ma_{1D}}$. An energy scale is given by the binding energy of the contact interaction $\varepsilon = \dfrac{\hbar^2}{ma_{1D}^2}$. To obtain the equation of state at a finite temperature $t = k_BT/\varepsilon$ (from now on we put $\varepsilon = 1$) we numerically solve a truncated set of the thermodynamic Bethe ansatz equations[12,34], given by two nonlinear integral equations

$$\varepsilon(k) = 2(k^2 - \mu - \frac{E_B}{4\varepsilon}) + \frac{t}{\pi}\int_{-\infty}^{\infty}\frac{dq}{1+(k-q)^2}\ln(1+e^{-\varepsilon(q)/t}) + \frac{2t}{\pi}\int_{-\infty}^{\infty}\frac{dq}{1+4(k-q)^2}\ln(1+e^{-\kappa(q)/t})$$

$$\kappa(k) = k^2 - \mu - h + \frac{2t}{\pi}\int_{-\infty}^{\infty}\frac{dq}{1+4(k-q)^2}\ln(1+e^{-\varepsilon(q)/t})$$

where $\mu = \dfrac{\mu_1+\mu_2}{2}$ and $h = \dfrac{\mu_1-\mu_2}{2}$. We have modified the original equations by replacing the binding energy of the contact interaction with the true two-body binding energy $E_B$ in a harmonic waveguide in order to have the proper definition for the chemical potentials. Densities $n_{1,2}$ are obtained from the solution of two coupled linear integral equations[35] (similar to the equations for the zero-temperature Bethe ansatz)

$$(1+e^{\varepsilon(k)/t})\sigma(k) = \frac{1}{\pi} - \frac{1}{\pi}\int_{-\infty}^{\infty}\frac{dq\sigma(q)}{1+(k-q)^2} - \frac{2}{\pi}\int_{-\infty}^{\infty}\frac{dq\rho(q)}{1+4(k-q)^2}$$

$$(1+e^{\kappa(k)/t})\rho(k) = \frac{1}{2\pi} - \frac{2}{\pi}\int_{-\infty}^{\infty}\frac{dq\sigma(q)}{1+4(k-q)^2}$$

as

$$n_2a_{1D} = 2\int_{-\infty}^{\infty}dk\sigma(k)$$

$$(n_1-n_2)a_{1D} = 2\int_{-\infty}^{\infty}dk\rho(k)$$

This truncation is accurate when thermal fluctuations are unable to break the tightly bound pairs, that is, when $k_BT/\varepsilon \ll 1$ (for a detailed discussion of a similar approximation see ref. 36). In the experiment, $k_BT/\varepsilon \approx 0.02$–$0.03$, and we explicitly checked that the higher-order terms in the thermodynamic Bethe ansatz equations are small. Confinement effects[37–39] can modify the interactions between pairs and excess fermions in a way not captured by the Gaudin–Yang model. A study of the three- and four-body problem carried out in ref. 40 shows that for our experimental parameters, $a_\perp/a_{3D} \approx -0.19$, these confinement effects shift energies by ~10%.

At strong coupling ($n^{1D}a_{1D} \to 0$), the equation of state of the Gaudin–Yang model reduces to that of a Tonks gas of bosons and a free Fermi gas[6,7]. This simplicity hides the fact that there are FFLO correlations in the system, with the many-body wavefunction changing sign whenever a boson crosses a fermion (see Supplementary Information).

**Calculation of density profiles.** For each tube, we use the Thomas–Fermi local density approximation to calculate the 1D density profiles, but allow the chemical potential to vary arbitrarily from one tube to the next

$$n_\sigma^{1D}(\rho,z) = n_\sigma^{1D}(\mu^c(\rho) - \frac{1}{2}m\omega_z^2z^2, h(\rho), t)$$

where $\sigma = 1, 2$. $\mu^c(\rho)$, $h(\rho)$ are related to the particle numbers for a tube a distance $\rho$ from the central axis by

$$N_\sigma(\rho) = \int_{-\infty}^{\infty}dz n_\sigma^{1D}(\mu^c(\rho) - \frac{1}{2}m\omega_z^2z^2, h(\rho), t)$$

Numerically inverting this equation, we find the central chemical potentials $\mu^c(\rho)$, $h(\rho)$. Then $N_\sigma(\rho)$ is obtained from the experimental data by inverse Abel transforming the radial profiles

$$n_{r,\sigma}(y) = \int_{-\infty}^{\infty}dz n_{c,\sigma}(y,z) = \frac{4}{\lambda^2}\int_{-\infty}^{\infty}dx N_\sigma(\sqrt{x^2+y^2}) \text{ through}$$

$$N_\sigma(\rho) = -\frac{\lambda}{4\pi}\int_{\rho}^{\infty}dy\frac{\partial_y n_{\gamma,\sigma}(y)}{\sqrt{y^2-\rho^2}}$$

where $n_{c,\sigma}(y,z) = \dfrac{4}{\lambda^2}\displaystyle\int_{-\infty}^{\infty}dx n_\sigma^{1D}\left(\sqrt{x^2+y^2}, z\right)$ is the column density. We fit the radial densities $n_{r,\sigma}(y)$ to a simple functional form, and analytically perform the integrals. We use the extracted $N_\sigma(\rho)$ to normalize our radii in Fig. 3.


31. Bergeman, T., Moore, M. G. & Olshanii, M. Atom-atom scattering under cylindrical harmonic confinement: numerical and analytic studies of the confinement induced resonance. *Phys. Rev. Lett.* **91,** 163201 (2003).
32. Kinast, J. *et al.* Heat capacity of a strongly interacting Fermi gas. *Science* **307,** 1296–1299 (2005).
33. Gaudin, M. Un systeme a une dimension de fermions en interaction. *Phys. Lett. A* **24,** 55–56 (1967).
34. Yang, C. N. Some exact results for the many-body problem in one dimension with repulsive delta-function interaction. *Phys. Rev. Lett.* **19,** 1312–1315 (1967).

35. Takahashi, M. One-dimensional electron gas with delta-function interaction at finite temperature. *Prog. Theor. Phys.* **46,** 1388–1406 (1971).
36. Zhao, E., Guan, X.-W., Liu, W. V., Batchelor, M. T. & Oshikawa, M. Analytic thermodynamics and thermometry of Gaudin-Yang Fermi gases. *Phys. Rev. Lett.* **103,** 140404 (2009).
37. Heidrich-Meisner, F., Feiguin, A. E., Schollwoeck, U. & Zwerger, W. The BCS-BEC crossover and the disappearance of FFLO-correlations in a spin-imbalanced, one-dimensional Fermi gas. *Phys. Rev. A* **81,** 023629 (2010).
38. Mora, C., Egger, R., Gogolin, A. O. & Komnik, A. Atom-dimer scattering for confined ultracold fermion gases. *Phys. Rev. Lett.* **93,** 170403 (2004).
39. Baur, S. K., Shumway, J. & Mueller, E. J. FFLO vs Bose-Fermi mixture in polarized 1D Fermi gas on a Feshbach resonance: a 3-body study. *Phys. Rev. A* **81,** 033628 (2010).
40. Blume, D. & Rakshit, D. Excitation spectrum and effective interactions of a highly elongated Fermi gas. *Phys. Rev. A* **80,** 013601 (2009).